INTERNATIONAL JOURNAL OF CLIMATOLOGY
Int. J. Climatol. **36**: 4929–4941 (2016)
Published online 19 February 2016 in Wiley Online Library
(wileyonlinelibrary.com) DOI: 10.1002/joc.4681

RMetS
Royal Meteorological Society

The surface climatology of the Ross Ice Shelf Antarctica

Carol A. Costanza,[a]* Matthew A. Lazzara,[a,b] Linda M. Keller[a,c] and John J. Cassano[d]

[a] *Antarctic Meteorological Research Center, Space Science and Engineering Center, University of Wisconsin-Madison, Madison, WI, USA*
[b] *Department of Physical Sciences, School of Arts and Sciences, Madison Area Technical College, Madison, WI, USA*
[c] *Department of Atmospheric and Oceanic Sciences, University of Wisconsin-Madison, Madison, WI, USA*
[d] *Department of Atmospheric and Oceanic Sciences, Cooperative Institute for Research in Environmental Sciences, University of Colorado-Boulder, Boulder, CO, USA*

ABSTRACT: The University of Wisconsin-Madison Antarctic Automatic Weather Station (AWS) project has been making meteorological surface observations on the Ross Ice Shelf (RIS) for approximately 30 years. This network offers the most continuous set of routine measurements of surface meteorological variables in this region. The Ross Island area is excluded from this study. The surface climate of the RIS is described using the AWS measurements. Temperature, pressure, and wind data are analysed on daily, monthly, seasonal, and annual time periods for 13 AWS across the RIS. The AWS are separated into three representative regions – central, coastal, and the area along the Transantarctic Mountains – in order to describe specific characteristics of sections of the RIS. The climatology describes general characteristics of the region and significant changes over time. The central AWS experiences the coldest mean temperature, and the lowest resultant wind speed. These AWSs also experience the coldest potential temperatures with a minimum of 209.3 K at Gill AWS. The AWS along the Transantarctic Mountains experiences the warmest mean temperature, the highest mean sea-level pressure, and the highest mean resultant wind speed. Finally, the coastal AWS experiences the lowest mean pressure. Climate indices (MEI, SAM, and SAO) are compared to temperature and pressure data of four of the AWS with the longest observation periods, and significant correlation is found for most AWS in sea-level pressure and temperature. This climatology study highlights characteristics that influence the climate of the RIS, and the challenges of maintaining a long-term Antarctic AWS network. Results from this effort are essential for the broader Antarctic meteorology community for future research.

KEY WORDS climate; Antarctica; meteorology; Ross Ice Shelf

Received 20 September 2015; Revised 18 December 2015; Accepted 12 January 2016

1. Introduction

Using Automatic Weather Station (AWS) data for climate studies in the Antarctic is not a new concept. Other nations have their own network of AWS and have done various regional climatologies of Antarctica. The Australian National Antarctic Research Expedition (ANARE) has installed an AWS network mostly in East Antarctic, and the British Antarctic Survey (BAS) has installed an AWS network mostly in the peninsula region of Antarctica. A climatology of East Antarctica was completed by Allison *et al.* (1993) by using AWS. Similarly, BAS has conducted studies using AWS data for model comparison in climatologies of the whole continent (Van Lipzig *et al.*, 2004; Turner *et al.*, 2005). Wisconsin's Antarctic AWS network is mainly installed in West Antarctica and the Ross Ice Shelf/Ross Sea region, along with several stations on the High Polar Plateau. The Ross Ice Shelf (RIS) in Antarctica is a unique region bordered on the west and south by the Transantarctic Mountains, on the north by the Ross Sea, and on the east by the West Antarctic Ice Sheet. Barrier winds, katabatic winds, mesocyclones, and synoptic scale cyclones are frequent phenomena in the area, and they interact to produce the Ross Ice Shelf air stream (RAS; Parish *et al.*, 2006; Seefeldt and Cassano, 2012; Nigro and Cassano, 2014). The RAS has a pronounced warming effect at the surface of the RIS (Coggins *et al.*, 2014). Mesocyclones and synoptic scale cyclones in the RIS area have been studied in detail by Carrasco *et al.* (2003), Cohen *et al.* (2013), and Steinhoff *et al.* (2013). As this is one of the most active mesocyclogenetic regions of the world, these cyclones have a large impact on the RAS (Parish *et al.*, 2006).

Two aspects of the climate of the RIS that are impacted by terrain, barrier, and katabatic winds have been widely studied. Barrier winds are due to the piling up of stable air moving from the east towards the Transantarctic Mountains (Schwerdtfeger, 1984). This wind is created when the pressure gradient force is directed perpendicular and away from the mountains, creating a strong flow along the mountains, which is somewhat deflected to the east due to surface friction (Schwerdtfeger, 1984; Seefeldt *et al.*, 2007). Barrier winds are found to be particularly strong when there is a high-pressure system at the base of the mountains, creating separate regions of high pressure along the barrier (Nigro *et al.*, 2012; Nigro and Cassano

* Correspondence to: C. Costanza, Antarctic Meteorological Research Center, Space Science and Engineering Center, University of Wisconsin-Madison, 1225 West Dayton Street, Madison, WI 53706, USA. E-mail: carol.costanza@ssec.wisc.edu

2014). Katabatic winds, which are due to negatively buoyant air or high-density cold air, descend adiabatically down the glaciers in the Transantarctic Mountains (Bromwich, 1989). The adiabatic warming due to the descending air and turbulent mixing of the surface inversion due to the strong winds, produces warm signatures in infrared satellite images that can be verified using AWS (Bromwich and Carrasco, 1992).

Larger scale modes of climate variability have been shown to impact Antarctic weather and climate. El Nino Southern Oscillation (ENSO) occurs when sea surface temperatures become anomalously warm or cold creating a global effect on the climate (Turner, 2004; Welhouse *et al.*, 2016). Studies for the Southern Hemisphere explain that the atmospheric forcing leads the sea surface temperature anomaly by one whole season (Jin and Kirtman, 2009). The semiannual oscillation (SAO) also has a large impact on the climate of Antarctica due to increased cyclonic activity during the equinoxes. Then, the circumpolar jet moves closer to the poles, and due to rapid heating and cooling rates on the continent as opposed to the oceans, an SAO is found in pressure and wind (Van Loon, 1966; Meehl, 1991; Simmonds and Jones, 1998; Van den Broeke, 1998a, 1998b). A third large-scale forcing comes from the southern annular mode (SAM; Marshall, 2003, 2007). The phase of SAM indicates the strength of the westerlies and whether they are close to Antarctica or have moved farther north.

The Wisconsin AWS program began installing weather stations in Antarctica in 1980 (Stearns *et al.*, 1993; Lazzara *et al.*, 2012a) and by 1987, eight AWS were installed on the RIS. Today, there are 14 AWSs found across the RIS region. Thus, there are roughly 25–30 years of daily data from a selection of AWS for this unique area. The AWSs used for this study were chosen to maximize the spatial and temporal coverage over the entire RIS. The AWSs include: Gill, Schwerdtfeger, Lettau, and Margaret in the central RIS; Elaine, Eric, Marilyn, Mary, Meeley, and Sabrina along the Transantarctic Mountains or in the western RIS; Nascent, Martha II, and Vito in the northern coastal region of the RIS (Figure 1). These three regions were chosen to examine the effects of terrain and distance to the ice edge on the climate of the RIS. For this study, measurements such as temperature, potential temperature, pressure, wind speed, wind direction, and resultant wind are utilized to understand the climate of the RIS.

Most climatology studies of the area have concentrated on specific stations, regions, or the whole continent (Turner *et al.*, 2005). This study will examine the climate of the entire RIS using AWS observations. Stations have been chosen for their long temporal record as well as to represent the various regions of the RIS. This effort excludes the Ross Island region, which has been separately studied (Nylen *et al.*, 2004; Monaghan *et al.*, 2005; Bernhard *et al.*, 2006). Section 2 describes the AWS data set and methods used to conduct the climatology study. Section 3 examines the results for each parameter measured by the AWS and how the annual as well as seasonal climate varies by region. Section 4 discusses AWS movement, instrument improvement, and winter data gaps. Finally, Section 5 explains the significant results and future work.

2. Data and methods

The data used for this project are observations from the University of Wisconsin-Madison Antarctic Automatic Weather Station network (Figure 1 and Table 1). The AWS primarily transmits observational data via the Argos satellite data collection system. From this platform, the data are relayed in real-time to forecasters, researchers, and modelling centres via the Global Telecommunications System (Lazzara *et al*., 2012a). The observations are also available in real time from the Internet via the web or local data manager (LDM) relay, often within 2 h of the observational time. A complete collection of AWS transmissions is provided by Argos to project personnel on a monthly basis. With that collection, a rigorous quality control (QC) process begins (Lazzara *et al*., 2012a). Historically, over the period 1980–2000, this process involved an intensive manual gross and fine error check, which consisted of a set of limits for each variable where the values outside of the limits were considered errors. Since 2000, the QC process now employs a specially designed program written in the Interactive Data Language software to set the limits to 2 SD from the mean in a centred moving window comprising seventy-two 10-min observations. This semi-automates much of the labour-intensive QC, yet allows a scientist to manually look at any parameter in the time series to compare errors to the rest of the observations. Observations that the QC program marks as errors can be retained if there is corroborating evidence and the scientist thinks they are correct. Once the QC process is complete, monthly summaries of the observations can be made for each AWS site, along with three-hourly, hourly, and 10 min data.

The monthly summaries contain the mean, maximum, and minimum values for temperature and pressure, the resultant wind speed and direction, the maximum wind speed and direction, and constancy of the wind. The constancy of the wind is defined as the ratio of the monthly mean vector wind speed to the scalar wind speed. All of the mean parameters are calculated using the three-hourly quality controlled observations, and the maximum and minimum parameters are calculated using the 10-min observations. The information from these monthly summaries was the starting point for this climatology study.

To construct a more detailed data set than the monthly summaries, the three-hourly quality controlled observations were utilized for each AWS. Using three-hourly observations of temperature, pressure, wind speed, and wind direction, the mean, maximum, and minimum of each variable were determined for each station for the whole operational period of each AWS. Sea-level pressure was calculated using the hypsometric equation with station pressure observations and the corresponding station temperature observations. These variables were evaluated using daily mean values from the eight observations per day in each station's operational period, ranging from 4 to

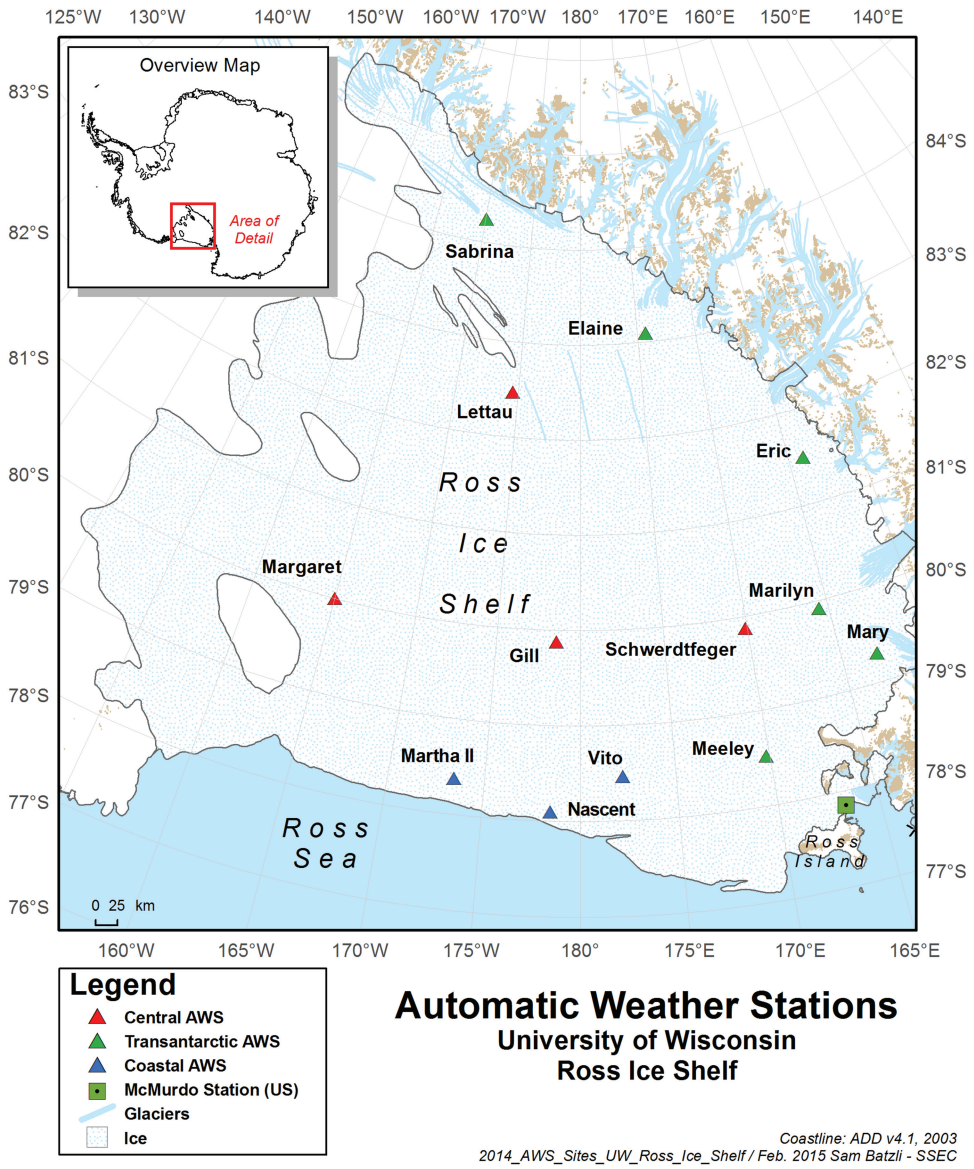

Figure 1. A map of the Ross Ice Shelf shows the locations of the AWS sites used in this project-orientated Greenwich up and north is down. Central AWSs are in red, coastal AWSs are in blue, and Transantarctic Mountain AWSs are in green.

29 years (Table 1). Potential temperature was calculated using the three-hourly observations for both temperature and pressure, and then a minimum value was calculated for all AWS.

One concern was found in Nascent AWS wind data because the orientation was not consistent with the other AWS wind data; therefore, Nascent AWS wind data were eliminated from this study. This issue is likely caused by the movement of Nascent AWS on the northern edge of the RIS (Brunt *et al.*, 2010). Only the temperature and pressure data from Nascent AWS were utilized for this study.

Student *t*-Tests were used to assess the significance of an increase or decrease of a variable over time. These tests were completed for temperature and sea-level pressure annually and seasonally, for the four AWS with the longest operational periods (years): Gill (29), Lettau (26), Marilyn (30), and Schwerdtfeger (29). Significance at the 95% confidence level was only valid if an AWS's annual or seasonal data set contained at least 20 years of data. Then, least-squares linear regressions were created to determine the linear rate of change with time (slope) and the standard error for the estimated rate. The difference in the calculated slope and the confidence interval is the standard error calculation. Thus, this creates a more descriptive data set of the climate about the increase or decrease of different parameters of the RIS climate.

Finally, the multivariate ENSO index (MEI), SAM, and SAO were tested for significant correlation against temperature and sea-level pressure. The wind data set was determined to be too short for this type of correlation. The MEI is used to monitor ENSO using six variables over the Pacific Ocean (Wolter and Timlin, 1993). These six variables are: sea-level pressure, zonal and meridional components of the surface wind, sea surface temperature, surface air temperature, and total cloudiness fraction of the sky. The SAM is the dominant mode for the Southern

Table 1. The latitude, longitude, and elevation for the 13 AWS.

Station	Latitude	Longitude	Elevation (m)	Operational period (# of years)
Gill	79.879°S	178.565°W	53	1985–2013 (29)
Lettau	82.475°S	174.587°W	38	1986–2011 (26)
Margaret	80.000°S	165.000°W	67	2009–2013 (5)
Schwerdtfeger	79.875°S	170.105°E	54	1985–2013 (29)
Elaine	83.094°S	174.285°E	58	1986–2013 (28)
Eric	81.496°S	163.947°E	45	2005–2013 (9)
Marilyn	79.921°S	165.550°E	63	1984–2013 (30)
Mary	79.305°S	162.985°E	58	2005–2011 (7)
Meeley	78.520°S	170.180°E	49	1980–1985 (6)
Sabrina	84.247°S	170.068°W	88	2009–2013 (5)
Martha II	78.380°S	173.420°W	18	1987–1992 (6)
Vito	78.416°S	177.7823°E	49	2004–2013 (10)
Nascent	78.103°S	178.474°W	30	2004–2011 (8)

Hemisphere in terms of atmospheric variability (Marshall, 2003). SAM implies a major shift in the broad scale climate of the hemisphere. The bi-monthly MEI and monthly SAM indices were tested for significance by correlating the bi-monthly MEI and monthly SAM index values to the bi-monthly and monthly AWS temperature and sea-level pressure data, for those AWS with an operational period of at least 10 years. The significance of the correlation was calculated using the sampling theory of correlation with a Student *t*-test at the 95% confidence level. This was done in order to independently calculate the degrees of freedom. The SAO is a twice-yearly contraction and expansion of the circumpolar jet producing a wave in baroclinicity and depression activity (Van den Broeke, 2000). The second harmonic of temperature and sea-level pressure was used to visually depict the signature of the SAO. Together, these three climate forcings were utilized to examine the influence of the larger scale circulation on the climate of the RIS.

One issue that was discovered was the large amount of missing data from the AWS during the winter seasons. This often occurred when the voltage from the batteries became too low to power the AWS or strong weather systems damaged the AWS. In this case, a whole season is not contributing to the annual mean; therefore, the annual mean becomes incorrectly anomalous. In order to solve this issue, the daily missing mean values were replaced by the corresponding daily mean values calculated over the full record of each AWS if the number of days missing in a given year was <60 days, otherwise the annual mean was eliminated from the data set. The data replacement was done to preserve the annual mean without eliminating the data for the entire year. For seasonal means, the level of contribution to the seasonal mean was not as many days as the annual means. The daily missing mean values were replaced by the corresponding daily mean values calculated over the full record of each AWS if the number of days missing was <40 days for winter or 25 days for summer, autumn, and spring, or more than 40% in each season (defined in 3a). The two methods for modifying annual and seasonal means was the best way to try and preserve as much of the data as possible.

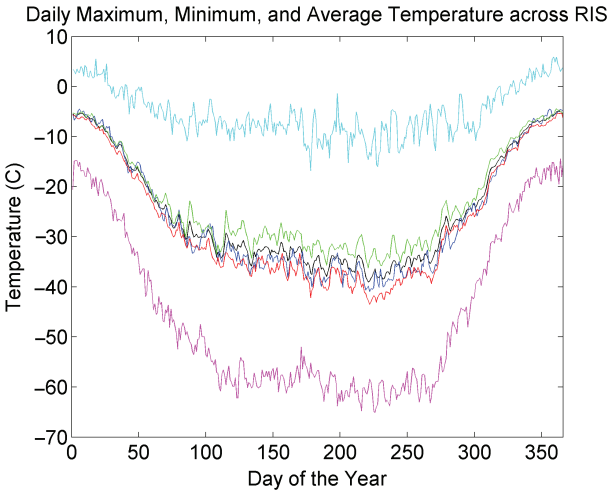

Figure 2. Daily maximum (cyan), mean (black), and minimum (magenta) temperature for the operational period of the 13 AWSs. Daily central RIS AWS mean (red), transantarctic RIS AWS mean (green), and coastal RIS AWS mean (blue) temperature for the operational period of each RIS region.

3. Results

3.1. Temperature

The long-term daily mean temperatures of all 13 stations across their operational periods are shown in Figure 2 in black. The mean temperatures vary from about −5 °C in the summer to about −35 °C in the winter. Figure 2 also shows the daily extreme maximum and minimum temperatures of all 13 stations across their operational periods. The mean maximum temperature is −5.1 °C and the mean minimum temperature is −45.4 °C. The greater difference in maximum and minimum temperatures in winter displays the greater temperature variability in the Antarctic winter seasons due to the intrusion of synoptic scale weather systems. The minimum temperature recorded on the RIS is −65.4 °C at Gill AWS on 14 August 2001, and the maximum temperature is 6.2 °C at Schwerdtfeger AWS on 26 December 2011 (Table 2).

The second harmonic fit to RIS mean daily temperature (Figure 3) demonstrates that there are two separate winter

Table 2. The maximum temperature, minimum temperature, maximum sea-level pressure, minimum sea level pressure, maximum wind speed, and potential temperature for all 13 AWSs given in month year.

Station	Maximum Temperature (°C)	Minimum Temperature (°C)	Maximum Pressure (hPa)	Minimum Pressure (hPa)	Maximum Wind Speed (m s^{-1})	Minimum Potential Temperature (K)
Gill	3.9, Dec 2005	−65.4, Aug 2001	1032.5, Jun 1999	928.6, Aug 2007	25.0, Jun 2007	209.3, May 2001
Lettau	4.9, Jan 2005	−63.1, Aug 2008	1033.2, Jun 1999	932.0, Jul 2006	31.0, Jun 2007	210.4, Sep 2009
Margaret	0.6, Nov 2011	−63.9, Jul 2010	1022.1, Aug 2011	945.5, May 2012	19.0, Jul 2011	211.1, Aug 2009
Schwerdtfeger	6.2, Dec 2011	−63.1, Jul 2004	1031.6, Jun 1999	934.7, Mar 1994	27.4, Jul 2011	211.1, Jul 2004
Elaine	3.6, Dec 1995	−62.1, Aug 2001	1039.4, Jun 1999	935.4, Jul 2006	33.2, Jul 1988	211.1, Sep 1998
Eric	4.6, Dec 2012	−62.4, Sep 2009	1029.6, Aug 2011	938.4, Jul 2006	28.7, Aug 2011	215.0, Sep 2011
Marilyn	4.9, Dec 2011	−58.5, Sep 2009	1034.4, Jun 1999	940.5, Jul 1993	33.8, Jul 1988	214.7, Sep 2009
Mary	4.1, Dec 2011	−58.6, Sep 2009	1031.0, Aug 2011	945.3, Jul 2006	26.4, Aug 2009	215.2, Sep 2010
Meeley	0.4, Dec 1982	−57.2, Jul 1985	1032.2, Aug 1981	948.5, Apr 1984	29.1, Apr 1981	218.2, Apr1981
Sabrina	1.7, Dec 2010	−57.8, Sep 2009	1025.0, Jun 2012	934.7, Sep 2010	35.4, Jul 2011	216.1, Sep 2009
Martha II	2.5, Dec 1989	−64.8, Aug 1990	1020.3, May 1990	934.9, Aug 1987	22.6, Aug 1987	210.2, Aug 1990
Vito	6.1, Dec 2011	−60.6, Aug 2008	1032.2, Jul 2007	944.8, Aug 2007	25.7, Jul 2011	213.5, Sep 2011
Nascent	0.9, Dec 2004	−54.9, Aug 2009	1024.7, Jul 2008	947.0, Aug 2008	24.2, Aug 2008	218.8, Nov 2011

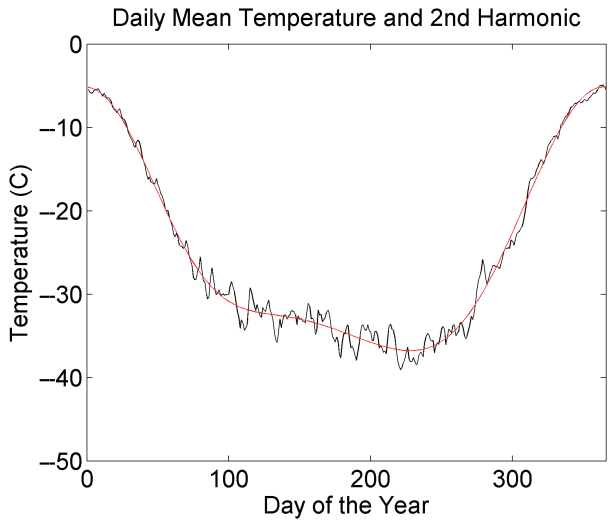

Figure 3. Daily RIS mean temperature (black) fit to the second harmonic (red).

seasons. The two winter seasons are well defined because the mean temperatures for Winter 1 in April, May, and June (Julian days 91–181) are between −30 and −40 °C, and temperatures for Winter 2 in July, August, and September (Julian days 182–273) are between −35 and −45 °C. The coldest days are during August in the middle of the second winter season. The RIS daily mean temperature time series vary from coastal stations in Antarctica, which have been characterized as coreless (Wendler and Kodama, 1993; Lazzara *et al*., 2012b).

Larger scale climate indices were correlated with the temperature data from four AWS to test for significant relationships. The temperatures for all four AWS were not significantly correlated with the MEI index using the sampling theory of correlation with a Student *t*-test at the 95% confidence level. The temperatures for the same four AWS were significantly correlated with the SAM index using the same analysis as the MEI index. Finally, the second harmonic of the Gill daily mean temperatures (Figure 3) was created to show the influence of the SAO on the daily temperatures throughout the year. Note especially the pause in the cooling and the quick warming of the daily mean temperatures in late winter or early fall about day 275, which coincides approximately with the equinox (Van Loon, 1966).

Station temperature was also analysed on a seasonal time scale. Figure 4(a) shows the seasonal temperature profiles for each of the 13 AWS across their operational period. During summer, all of the monthly mean AWS temperatures range from −5 to −10 °C versus winter 2 where all of the AWS temperatures range from −25 to −45 °C. Summer temperatures vary less interannually than winter temperatures due to higher synoptic cyclone activity in winter, which produces frequent departures from the monthly mean temperature (Cohen *et al*., 2013).

Annual mean temperature was also calculated for all 13 stations. When calculating the annual means, corresponding long-term daily average temperatures for each AWS were substituted for missing data points for years with <60 days missing. The annual mean temperatures range between −30 and −20 °C (Table 3). Figure 4(b) shows the annual mean temperature for four AWS and indicates minima in annual mean temperature in 2004 and 2010. These years correspond to central tropical Pacific El Nino events, which have a cooling effect in the RIS region during some months of the year (Wilson *et al*., 2014). Section 3.3 explores the ENSO events further.

The three sections of the RIS each have separate temperature characteristics. The AWS in the centre of the ice shelf experiences the coldest temperature all year round. The annual mean for the central AWS is −27.1 °C (Table 3). The AWS on the northern edge of the shelf along the coast has temperatures that are very consistent between the three AWSs due to their close proximity to each other. The annual mean temperature for the coastal AWS is −26.1 °C. The annual mean temperature for the AWS along the Transantarctic Mountains is −23.1 °C, and this is the warmest region analysed here due to katabatic warming events and strong winds creating turbulent mixing that stops a strong surface inversion from forming (Carrasco

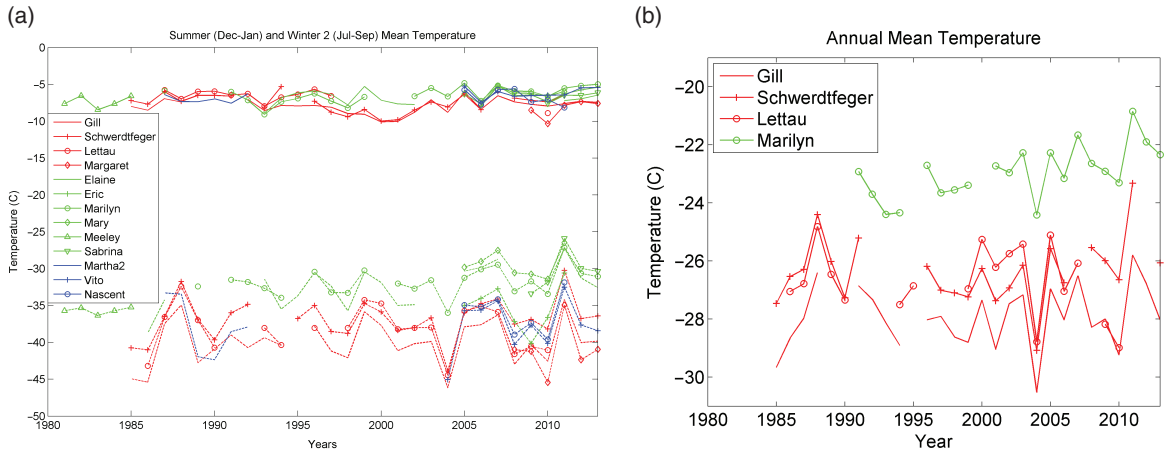

Figure 4. (a) Seasonal mean temperature (°C) for all 13 stations across their operational period for summer (Dec–Jan) in solid lines and winter 2 (Jul–Sep) in dashed lines. (b) Annual mean temperature (°C) for four AWSs across their operational period.

and Bromwich, 1993). The differences between the central and coastal AWS are not large. However, very different from other regions of the RIS, the AWS along the Transantarctic Mountains definitely experiences a warmer climate regime in terms of temperature.

Trends in the annual and seasonal mean temperature for the four AWSs with at least 20 years annually or seasonally were assessed and tested for significance using a Student *t*-test. Years were omitted from the time series if more than 60 days in a year were missing or there were <20 years of data available in a season. Significant increases in temperature are found at Marilyn AWS annually and during summer. Marilyn AWS experiences $+0.09\,^{\circ}\mathrm{C} \pm 0.06$ per year and $+0.09\,^{\circ}\mathrm{C} \pm 0.06$ per year during summer. The reasoning for high uncertainty is discussed in throughout Section 4.

3.2. Potential temperature

An atmospheric variable that has not been widely studied at the surface is potential temperature. Due to its low elevation, the RIS is an ideal location for achieving low potential temperatures. Figure 5 displays the minimum potential temperature recorded for each AWS. The AWS in the central area of the shelf experiences the coldest potential temperatures, indicated by the 210 K contour near Gill AWS. The minimum potential temperature recorded on the RIS was 209.3 K at Gill AWS on 19 May 2000, with a temperature at −65.1 °C and pressure at 979.3 hPa. The RIS is the area with the lowest potential temperatures in the AWS network, and likely in all of Antarctica.

3.3. Pressure

The long-term daily mean sea-level pressures of all 13 stations across their operational periods are shown in Figure 6 in black. The mean sea-level pressures vary from 975 to 995 hPa within a year. Figure 6 also shows that the mean maximum sea-level pressure is 1017.7 hPa and the mean minimum sea-level pressure is 955.5 hPa. The minimum sea-level pressure recorded on the RIS is 928.6 hPa at Gill AWS on 13 August 2007 and the maximum sea-level pressure is 1039.4 hPa at Elaine AWS on 17 June 1999 (Table 2).

Seasonal differences in sea-level pressure are an important aspect of the RIS. In general, mean daily sea-level pressure values are about 990 hPa, but there are two time periods that differ. Winter 1 (day 91–181) is characterized by higher sea-level pressure and spring (day 274–334) is characterized by lower sea-level pressure, which is depicted in Figure 7 utilizing the RIS annual mean sea level pressure. The shift in winter 1 reflects the amplification of the wave number 3 pattern as the strong polar vortex builds (Van den Broeke, 2000). The shift in the spring is consistent with the deepening of the circumpolar trough and Amundsen Sea low during spring (Fogt *et al.*, 2012; Turner *et al.*, 2013). Figure 8(a) shows the summer and winter 2 sea-level pressure trends for each of the 13 AWSs across their operational period.

Larger scale climate indices were correlated with AWS sea-level pressure data as well. All four AWSs (Gill AWS, Lettau AWS, Marilyn AWS, and Schwerdtfeger AWS) were significantly correlated to the MEI and SAM. Finally, the second harmonic of the RIS daily mean sea-level pressure plot was created to visually examine the effect of the SAO (Figure 7). Similar to the temperature SAO analysis, the RIS daily sea-level pressure shows a semiannual cycle similar to SAO. The sea-level pressure shift in spring reflects the SAO, which causes low-pressure systems to penetrate further south during the spring (Cohen *et al.*, 2013). For example, 1995, 2004, and 2010 show maxima in summer sea-level pressure yet minima in winter 2 pressure (Figure 8(a)), and sea-level pressure minima are found in the annual mean of four AWSs as well (Figure 8(b)). This even occurs in the Meeley AWS data from the early 1980s.

These types of seasonal sea-level pressure trends are consistent with the El Nino and La Nina pressure and temperature shifts. Specifically, the 2009–2010 El Nino event was unique due to the quick change from a Strong El Nino warm signal in the central Pacific, which rapidly decayed to a strong La Nina event within the autumn

Table 3. The summer, autumn, winter 1, winter 2, spring, and annual means for all 13 AWSs.

Station	Summer	Autumn	Winter 1	Winter 2	Spring	Annual
Gill	−8.0 °C	−23.4 °C	−36.2 °C	−40.0 °C	−22.6 °C	−27.9 °C
	990.5 hPa	990.3 hPa	988.8 hPa	986.2 hPa	983.0 hPa	987.8 hPa
	2.0 m s^{-1}	2.3 m s^{-1}	2.6 m s^{-1}	2.5 m s^{-1}	3.0 m s^{-1}	2.5 m s^{-1}
Lettau	−6.6 °C	−23.2 °C	−34.6 °C	−38.2 °C	−20.8 °C	−26.7 °C
	991.6 hPa	991.0 hPa	990.3 hPa	987.4 hPa	983.5 hPa	988.8 hPa
	2.3 m s^{-1}	1.8 m s^{-1}	2.3 m s^{-1}	2.3 m s^{-1}	3.0 m s^{-1}	2.2 m s^{-1}
Margaret	−8.9 °C	−24.1 °C	−37.7 °C	−40.6 °C	−22.6 °C	−28.8 °C
	988.3 hPa	986.0 hPa	985.1 hPa	983.6 hPa	979.6 hPa	984.4 hPa
	1.9 m s^{-1}	1.3 m s^{-1}	1.1 m s^{-1}	0.9 m s^{-1}	1.7 m s^{-1}	1.1 m s^{-1}
Schwerdtfeger	−7.6 °C	−23.2 °C	−33.7 °C	−36.8 °C	−21.1 °C	−26.4 °C
	990.5 hPa	990.2 hPa	989.9 hPa	987.6 hPa	983.1 hPa	987.8 hPa
	1.7 m s^{-1}	2.7 m s^{-1}	4.0 m s^{-1}	3.9 m s^{-1}	3.1 m s^{-1}	3.2 m s^{-1}
Elaine	−6.8 °C	−20.6 °C	−29.6 °C	−32.2 °C	−18.6 °C	−23.1 °C
	990.8 hPa	990.9 hPa	990.7 hPa	988.9 hPa	985.1 hPa	990.7 hPa
	1.5 m s^{-1}	2.5 m s^{-1}	3.0 m s^{-1}	2.6 m s^{-1}	2.7 m s^{-1}	2.5 m s^{-1}
Eric	−6.4 °C	−21.1 °C	−32.5 °C	−35.2 °C	−19.5 °C	−24.8 °C
	990.1 hPa	990.3 hPa	990.5 hPa	989.6 hPa	985.8 hPa	989.5 hPa
	1.0 m s^{-1}	1.3 m s^{-1}	1.6 m s^{-1}	1.6 m s^{-1}	1.7 m s^{-1}	1.4 m s^{-1}
Marilyn	−6.4 °C	−20.8 °C	−29.5 °C	−31.8 °C	−18.8 °C	−23.0 °C
	991.5 hPa	991.7 hPa	991.8 hPa	989.4 hPa	985.7 hPa	990.1 hPa
	1.6 m s^{-1}	3.5 m s^{-1}	5.5 m s^{-1}	5.7 m s^{-1}	3.4 m s^{-1}	4.2 m s^{-1}
Mary	−6.3 °C	−19.7 °C	−27.5 °C	−29.4 °C	−17.7 °C	−21.5 °C
	991.2 hPa	993.3 hPa	993.4 hPa	991.6 hPa	986.7 hPa	991.4 hPa
	1.5 m s^{-1}	3.4 m s^{-1}	5.0 m/s	4.6 m s^{-1} m s^{-1}	3.1 m s^{-1}	3.7 m s^{-1}
Meeley	−7.4 °C	−20.4 °C	−32.2 °C	−35.7 °C	−21.3 °C	−25.1 °C
	993.0 hPa	992.6 hPa	989.9 hPa	990.5 hPa	984.6 hPa	990.0 hPa
	3.1 m s^{-1}	4.8 m s^{-1}	5.6 m s^{-1}	4.7 m s^{-1}	5.0 m s^{-1}	4.7 m s^{-1}
Sabrina	−6.7 °C	−19.1 °C	−28.0 °C	−30.3 °C	−16.0 °C	−21.5 °C
	991.6 hPa	989.4 hPa	990.5 hPa	986.9 hPa	985.1 hPa	988.7 hPa
	3.2 m s^{-1}	4.7 m s^{-1}	5.9 m s^{-1}	5.9 m s^{-1}	6.7 m s^{-1}	5.3 m s^{-1}
Martha II	−7.0 °C	−23.7 °C	−34.8 °C	−37.8 °C	−23.2 °C	−27.1 °C
	986.6 hPa	984.5 hPa	985.2 hPa	980.7 hPa	978.8 hPa	983.1 hPa
	2.0 m s^{-1}	2.6 m s^{-1}	2.9 m s^{-1}	2.8 m s^{-1}	3.0 m s^{-1}	2.7 m s^{-1}
Vito	−6.2 °C	−21.1 °C	−34.2 °C	−37.7 °C	−21.4 °C	−26.1 °C
	990.5 hPa	990.9 hPa	989.6 hPa	988.5 hPa	984.4 hPa	988.8 hPa
	2.4 m s^{-1}	3.2m s^{-1}	3.9 m s^{-1}	3.6m s^{-1}	3.8 m s^{-1}	3.4 m s^{-1}
Nascent	−6.8 °C	−20.5 °C	−33.7 °C	−36.0 °C	−20.7 °C	−25.5 °C
	990.9 hPa	988.8 hPa	985.8 hPa	984.3 hPa	980.7 hPa	985.9 hPa

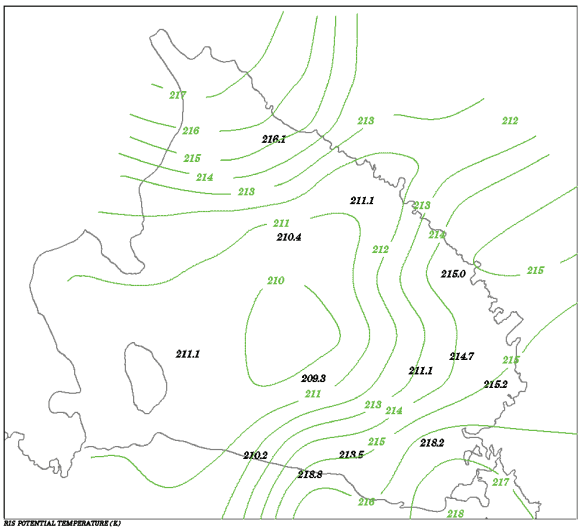

Figure 5. Thirteen AWSs minimum potential temperature (K) in grey and green contours of potential temperature.

and winter 1 of 2010 (Kim *et al*., 2011). This sea-level pressure shift between 2009 and 2010 can be seen in the change in the annual sea-level pressure means and is even more pronounced in the maximum sea-level pressure in the summer of 2010 and minimum sea-level pressure in winter 2 of 2010.

The three sections of RIS each have different sea level pressure features. The AWS on the coast of the ice shelf (blue) experience the lowest pressure all year round. The annual mean sea-level pressure for the central AWS is 988.1 hPa, yet the annual mean sea-level pressure for the coastal AWS is 984.6 hPa. The AWSs along the Transantarctic Mountains (green) experience katabatic and barrier winds; therefore, they are not only the warmest but they also have the highest pressure on the RIS. The annual mean sea-level pressure for the AWS along the Transantarctic Mountains is 990.1 hPa. A definite pressure gradient exists from the southwest corner of the RIS to the northeast corner of the RIS, which can be seen by the southeast to northwest orientated isobars in the eastern part of the RIS (Figure 9). The pressure pattern is commonly

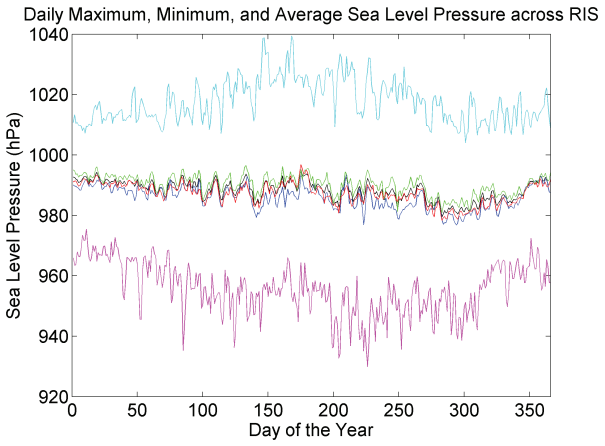

Figure 6. Daily maximum (cyan), mean (black), and minimum (magenta) sea-level pressure (hPa) for the operational period of the 13 AWSs. Daily central RIS AWS mean (red), transantarctic RIS AWS mean (green), and coastal RIS AWS mean (blue) sea-level pressure for the operational period of each RIS region.

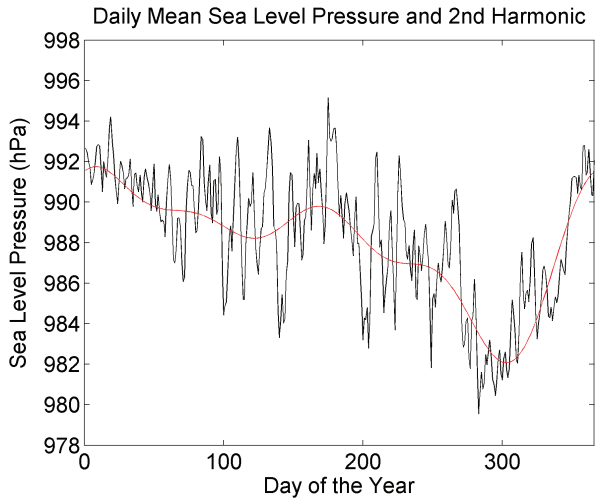

Figure 7. Daily RIS mean sea-level pressure (black) fit to the second harmonic (red).

found in AMPS forecasting geopotential heights distribution of mass (Parish *et al.*, 2006).

Similar to the temperature analysis, the annual mean sea-level pressure values were tested for significant increase or decrease over time using a Student *t*-test for the four AWS. Years were omitted from the time series if more than 60 days in a year were missing or there were <20 years of data available in a season. Significant sea-level pressure decreases were found at Gill AWS and Schwerdtfeger AWS both annually and seasonally. Specifically, Gill AWS experiences $-0.09\,\text{hPa} \pm 0.09$ per year, $-0.16\,\text{hPa} \pm 0.15$ per year during autumn, and $-0.16\,\text{hPa} \pm 0.16$ per year during winter 1. Schwerdtfeger AWS experiences $-0.16\,\text{hPa} \pm 0.13$ per year, $-0.22\,\text{hPa} \pm 0.15$ per year during autumn, and $-0.25\,\text{hPa} \pm 0.22$ per year during winter 1. These significant decreases in sea-level pressure do not correlate with significant changes in temperature at these AWSs. Both Gill and Schwerdtfeger are in the central area of the RIS, so there could be an increase in cyclones entering this region of the RIS causing a decrease in pressure over time. Similar decreases in pressure over a 50-year time scale were found over the whole of Antarctica (Turner *et al.*, 2005), and another study notes that there have been decreases in the number of cyclones yet those cyclones are deeper (Simmonds and Keay, 2000).

3.4. Wind

The long-term daily resultant wind speeds of all 13 AWS, except Nascent AWS, across their operational periods are shown in Figure 10 in black. The mean resultant wind speeds vary from about 1 to 5 m s^{-1} within a year. Figure 10 also shows the daily extreme maximum wind speeds with a mean maximum wind speed of 20.7 m s^{-1}. The maximum wind speed recorded for the AWS in this study is 35.4 m s^{-1} at Sabrina AWS on 27 July 2011 (Table 2).

Seasonal differences in wind are not as prevalent as other atmospheric parameters on the RIS. Wind speeds are highest during the winter seasons (Figure 8(a)), and wind speeds are the lowest during the summer with wind speeds <5 m s^{-1} on average for all AWS. Winter 2 displays the high wind speeds experienced specifically at Marilyn AWS during half of the year. Overall, there are higher resultant wind speeds at all of the AWS during the winters. Looking at the annual resultant wind speed for four AWSs (Figure 11), resultant wind speeds are highest at Marilyn AWS due to the proximity to the Transantarctic Mountains.

There are a few AWS that experience anomalously high and low wind speeds across the RIS. Wind roses for Sabrina AWS, Marilyn AWS, and Margaret AWS demonstrate the difference in wind speed and direction for these three different regions (Figure 12). Sabrina AWS experiences higher wind speeds at the southern edge of the shelf due to barrier winds (Nigro *et al.*, 2012). Marilyn AWS also experiences higher wind speeds due to katabatic winds in the northwest section of the RIS (Bromwich, 1989). Margaret AWS experiences lower wind speeds on the eastern part of RIS since this particular area is not affected by the RAS. Sabrina AWS wind has a constancy of 88% and is directed from the southeast, Marilyn AWS wind has a constancy of 80% and is directed from the southwest, and Margaret AWS wind has a constancy of 42% and is directed most often from the southeast but otherwise in many directions. Sabrina AWS and Marilyn AWS experience higher resultant wind speeds due to the higher constancy of persistent wind in those regions, versus the weaker wind at Margaret AWS.

Wind is analysed with respect to the three regions on the RIS. Figure 13 demonstrates the resultant wind speed and direction across the RIS with a well-defined RAS signature. The AWS in the central RIS experiences the lowest wind speeds with a resultant wind speed of 2.2 m s^{-1} and scalar wind speed of 4.1 m s^{-1}. The AWS along the coast experiences resultant wind speeds of 2.7 m s^{-1} and scalar wind speed of 4.4 m s^{-1}, similar to the central RIS. The AWS along the Transantarctic Mountains experiences the highest wind speeds with a resultant wind

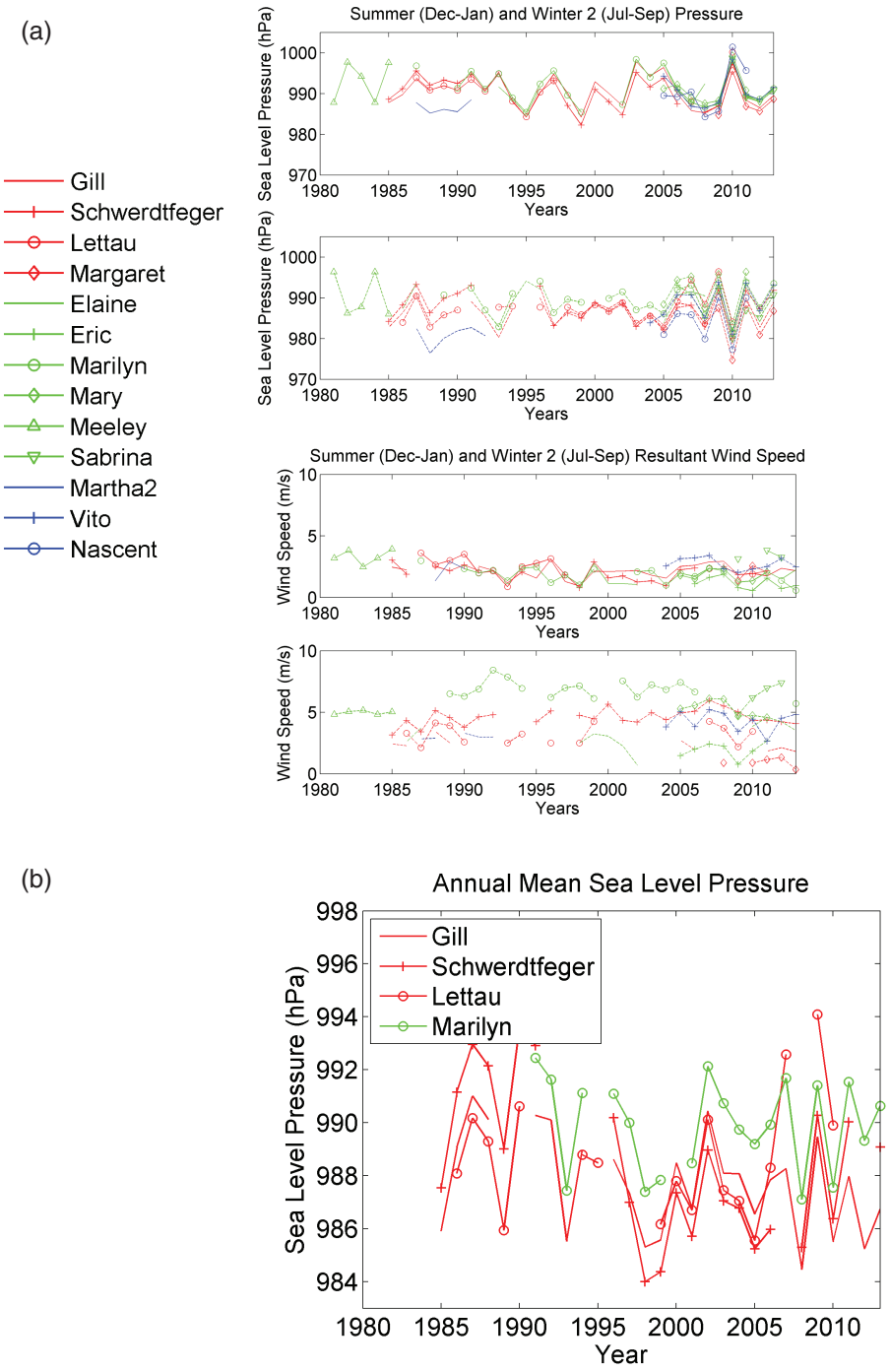

Figure 8. (a) Seasonal mean sea-level pressure (hPa) for all 13 AWSs across their operational period for summer (Dec–Jan) in solid lines and winter 2 (Jul–Sep) in dashed lines in the top two graphs, and the same for the bottom two graphs except for wind speed (m s^{-1}). (b) Annual mean sea-level pressure (mb) for four AWSs across their operational period.

speed of 3.4 m s^{-1} and scalar wind speed of 5.1 m s^{-1}. The wind direction in Figure 13 displays a distinct change in wind direction as you move north from southeasterly to southwesterly.

4. Discussion

4.1. AWS movements and instrument improvement

Although these AWSs are have not been moved by project personnel during their operational period, they are on a moving ice sheet and in a very harsh climate. Both of these issues come into play when analysing the climate of the RIS on long time scales. Global positioning system (GPS) coordinates from UNAVCO services are taken at nearly all of the AWS visits within the last decade. Thus, there are GPS coordinates for all of the AWS every couple of years. Based on latitude and longitude distance calculations, the AWS are moving ~0.3 km northeast per year in the southern regions of the RIS. Further north in the central region of the RIS AWS are moving ~0.5 km northeast per year, and

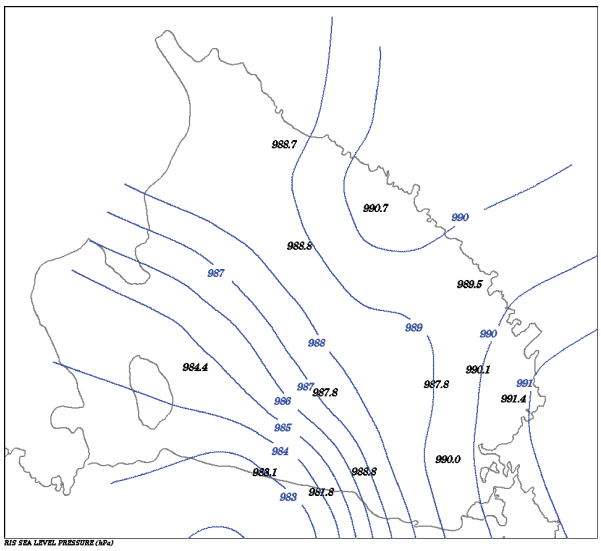

Figure 9. Mean sea-level pressure plotted for all 13 AWSs over their operational period in grey and blue contours of sea-level pressure.

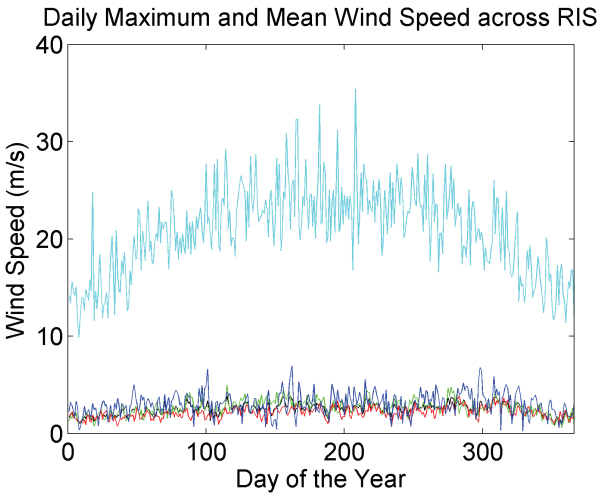

Figure 10. Daily maximum (cyan) and resultant (black) wind speed (m s^{-1}) for the operational period of the 13 AWSs except Nascent AWS. Daily central RIS AWS mean (red), transantarctic RIS AWS mean (green), and coastal RIS AWS mean (blue) resultant wind speed for the operational period of each RIS region.

even further north close to the RIS edge AWS are moving nearly 1 km northeast per year. Therefore, it is difficult to create an exact climatology of points that are moving horizontally slowly over time. Generally, the impact of this movement on climate records is minimal.

Movement of instrumentation is not only happening horizontally, but also vertically. On the RIS, net snow accumulation occurs. This can occur because of precipitation, evaporation, or snow blown into or away from the station area. Therefore, the AWS needs to be raised every few years in order for the instrumentation to stay above the level of the snow. On average, all of the AWS on the RIS get about 0.3 m of net accumulation per year. AWS in the northwest corner of the RIS, like Marilyn AWS, can get higher amounts of net accumulation closer to 0.5 m

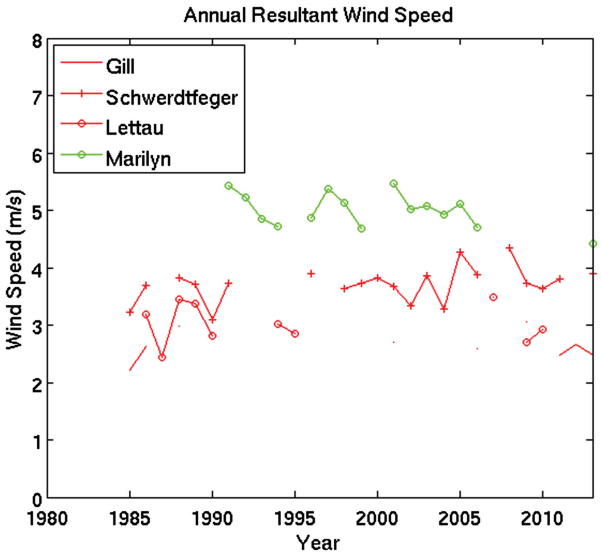

Figure 11. Annual resultant wind speed (m s^{-1}) for the operational period of four AWSs.

per year. Similar results were found using acoustic depth gauge measurements at AWS located in the northwest corner RIS and near Ross Island (Knuth *et al.*, 2009). The net snow accumulation at AWS adds to the challenge of creating a climatology by changing the distance of instruments to the surface. Instruments are always within the first 3 m above the surface, so differences in height due to accumulation are not large.

During the AWS visits, instrumentation is often improved, especially over a 30-year period. For instance, many AWSs are visited months after an instrument breaks, and then new instrumentation is installed. Thus, data from those months of downtime needed to be eliminated from the annual mean calculations. Since the beginning of the Antarctic AWS project, there have been many generations of hardware (Lazzara *et al.*, 2012a), which should be taken into account when comparing atmospheric variables. One other point worth noting is the two types of AWS electronics systems that have been developed at Wisconsin. The AWS2B is the older style system which started in the 1980s, and the AWSCR1000 is the newer style system which started in the 2010s (Table 4). In the general, most AWSs for this study were consistently either AWS2B or AWSCR1000 for the whole operational time period. Both Gill AWS and Lettau AWS were changed to AWSCR1000 in January 2011, and Schwerdtfeger changed to an AWSCR1000 in January 2013. During analysis, change points and spikes in parameters were taken into consideration for validity across all time scales of this study.

4.2. AWS winter and summer irregularities

AWSs in Antarctica are subjected to some of the most extreme weather on the planet. It is no surprise that during the winter months the AWS instrumentation, especially aerovanes, can malfunction due to the cold temperatures and high winds on the RIS. These winter failures lead to

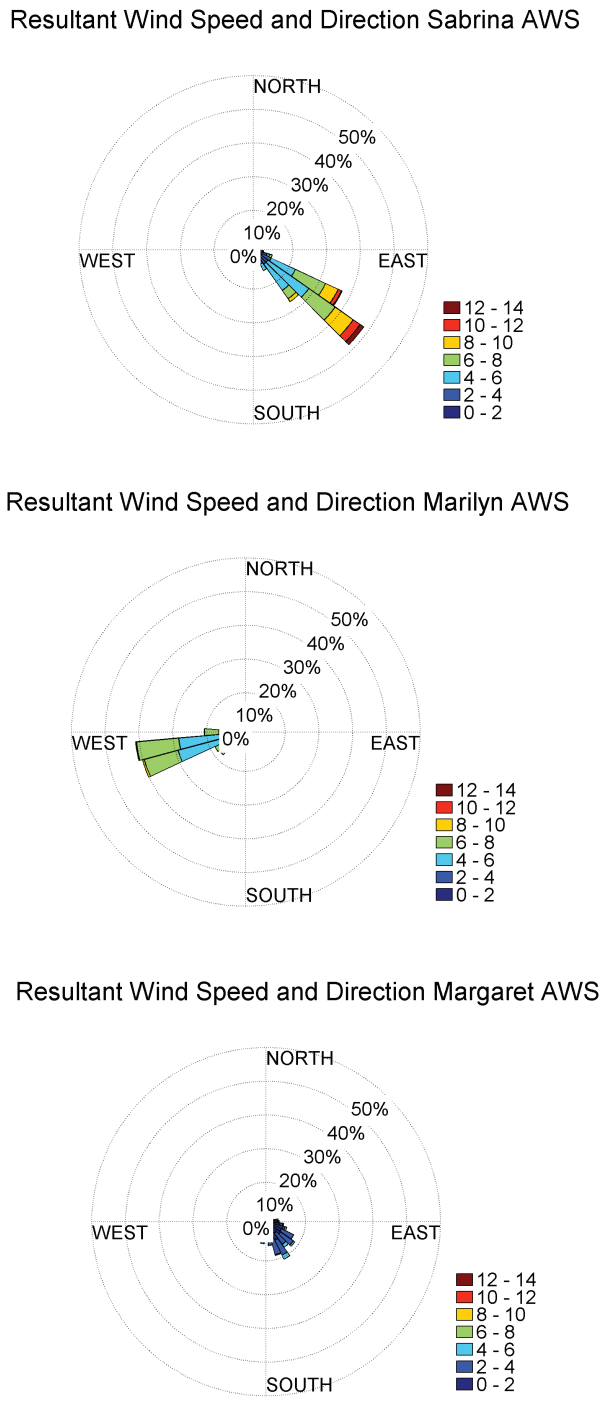

Figure 12. Resultant wind speed (m s^{-1}) and direction for Sabrina AWS (top), Marilyn AWS (centre), and Margaret AWS (bottom).

incorrect annual mean calculations, and therefore elimination of a year for annual calculations. For instance, the first 5 years after installation, Marilyn AWS had over 60 days of missing data. Those years were eliminated from annual mean calculations and statistical testing. If AWS stations had more consistent data with complete winter months, the statistical testing could have been more robust and potentially more significant. It is important to remember that these weather stations are run automatically and are only visited for maintenance every couple of years, so

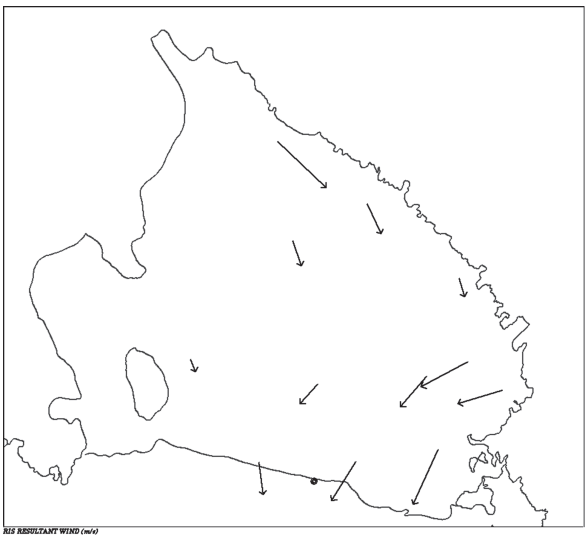

Figure 13. Twelve AWSs resultant wind speed vectors (m s^{-1}) pointed in the direction the wind is going to, where the magnitude of the vector is a factor of the resultant wind speed.

Table 4. The specific instruments used for measuring temperature, pressure, and wind speed for an AWS2B or AWSCR1000 system with accuracy in parentheses.

	AWS2B	AWSCR1000
Temperature	Weed PRT (±0.5 °C)	Campbell Scientific Model 43347 (±0.3 °C)
Pressure	Paroscientific Model 215A (±0.2 hPA)	Paroscientific Model 216B (±0.8 hPa)
Wind Speed	Bendix or Belfort (±0.5 m s^{-1})	RM Young Model 215A (±0.3 m s^{-1})

it is non-trivial to get the perfectly consistent data that scientists desire.

During the summer months in Antarctica, AWS are subject to continuous solar radiation. The solar radiation affects the temperature by warming the temperature shields and sensors and producing a temperature warmer than the ambient air temperature. Studies have shown that this is mostly a problem when winds are less than 4–6 m s^{-1} with high amounts of solar radiation (Genthon *et al.*, 2011). Corrections to temperature due to solar radiation heating have been made since the 2000s, and a more efficient radiation shield has been installed at many of the AWS. The older AWS data have also been examined for the stations used in this study.

5. Conclusion

Since the start of the Antarctic AWS project, nearly 30 years of AWS observations have been taken across all regions of the Antarctic. For this study, a climatology of the RIS is created using 13 AWSs. The climatology was examined over different time scales and different regions of the RIS analysing temperature, pressure, and wind.

The mean temperatures vary from −5 to −35 °C, mean sea-level pressures vary from 975 to 995 hPa, and mean resultant wind speeds are usually <5 m s^{-1}. The following significant annual trends were identified at three of the four AWSs with the longest operational period: a temperature increase of $+0.09 \pm 0.06$ °C per year (Marilyn AWS), a decrease in sea-level pressure of -0.09 ± 0.09 hPa per year (Gill AWS), and a decrease in sea-level pressure of -0.16 ± 0.13 hPa per year (Schwerdtfeger AWS). Based on the data set for this study, decreases in pressure at Schwerdtfeger AWS correlated with increases in wind speed over time. These four AWSs were significantly correlated in temperature and sea-level pressure with the MEI, SAO, and SAM.

General characteristics of the regions were identified. The central AWS experiences the coldest mean temperature, and lowest resultant wind speed. These AWSs also experience the coldest potential temperatures with a minimum of 209.3 K at Gill AWS. The AWS along the Transantarctic Mountains experiences the warmest mean temperature, the highest mean sea-level pressure, and the highest mean resultant and scalar wind speed. The coastal AWS experiences the lowest mean sea-level pressure.

The results of this climatology provide valuable information to Antarctic researchers to gain a better understanding of the RIS for their own research projects. The use of AWS proved to be challenging due to the large amounts of missing data, but in the end this study demonstrated a method for AWS-based climatologies. In the future, the Marilyn AWS temperature will be investigated for continued warming, and other regions of Antarctica could be analysed.

Acknowledgements

The authors appreciate the support of the Division of Polar Programs at the National Science Foundation, NSF grant numbers ANT-0944018, ANT-1141908, ANT-1245663, and ANT-1245737, for their support of the US Antarctic AWS Program and Antarctic Meteorological Research Center. This material is based on data, equipment, and/or engineering services provided by the UNAVCO Facility with support from the National Science Foundation (NSF) and National Aeronautics and Space Administration (NASA) under NSF Cooperative Agreement No. EAR-0735156. The authors thank the three anonymous reviewers whose comments and suggestion were helpful in the review process.

References

Allison I, Wendler G, Radok U. 1993. Climatology of the East Antarctic ice sheet (100°E to 140°E) derived from automatic weather stations. *J. Geophys. Res.* **98**: 8815–8823, doi: 10.1029/93JD00104.

Bernhard G, Booth CR, Ehramjian JC, Nichol SE. 2006. UV climatology at McMurdo Station, Antarctica, based on version 2 data of the National Science Foundation's Ultraviolet Radiation Monitoring Network. *J. Geophys. Res.* **111**: D11201, doi: 10.1029/2005JD005857.

Bromwich DH. 1989. Satellite analyses of Antarctic Katabatic wind behavior. *Bull. Am. Meteorol. Soc.* **70**: 738–749.

Bromwich DH, Carrasco JF. 1992. Satellite observations of Katabatic-wind propagation for great distances across the Ross Ice Shelf. *Mon. Weather Rev.* **120**: 1940–1949.

Brunt K, King MA, Fricker HA, MacAyeal DR. 2010. Flow of the Ross Ice Shelf, Antarctica, is modulated by the ocean tide. *J. Glaciol.* **56**: 157–161, doi: 10.3189/002214310791190875.

Carrasco JF, Bromwich DH. 1993. Satellite and automatic weather station analyses of katabatic surges across the Ross Ice Shelf. In *Antarctic Meteorology and Climatology: Studies Based on Automatic Weather Stations*. Antarctic Research Series No. 61, Bromwich DH, Stearns CR (eds). American Geophysical Union, Washington, DC, 93–108.

Carrasco JF, Bromwich DH, Monaghan AJ. 2003. Distribution and characteristics of mesoscale cyclones in the Antarctic: Ross Sea Eastward to the Weddell Sea. *Mon. Weather Rev.* **131**: 289–301.

Coggins JHJ, McDonald AJ, Jolly B. 2014. Synoptic climatology of the Ross Ice Shelf and Ross Sea region of Antarctica: k-mean clustering and validation. *Int. J. Climatol.* **34**: 2330–2348, doi: 10.1002/joc.3842.

Cohen L, Dean S, Renwick J. 2013. Synoptic weather types for the Ross Sea Region, Antarctica. *J. Clim.* **26**: 636–649, doi: 10.1175/JCLI-D-11-00690.1.

Fogt RL, Wovrosh AJ, Langen RA, Simmonds I. 2012. The characteristic variability and connection to the underlying synoptic activity of the Amundsen-Bellingshausen Seas Low. *J. Geophys. Res.* **117**: D07111, doi: 10.1029/2011JD017337.

Genthon C, Six D, Favier V, Lazzara M, Keller L. 2011. Atmospheric temperature measurement biases on the Antarctic Plateau. *J. Atmos. Oceanic Technol.* **28**: 1598–1605, doi: 10.1175/JTECH-D-11-00095.1.

Jin D, Kirtman BP. 2009. Why the Southern Hemisphere ENSO responses lead ENSO. *J. Geophys. Res.* **114**: D23101, doi: 10.1029/2009JD012657.

Kim W, Yeh S, Kim J, Kug J, Kwon M. 2011. The unique 2009–2010 El Nino event : a fast phase transition of warm pool El Nino to La Nina. *Geophys. Res. Lett.* **38**: L15809, doi: 10.1029/2011Gl048521.

Knuth SL, Tripoli GJ, Thom JE, Weidner GA. 2009. The Influence of blowing snow and precipitation on snow depth gauge across the Ross Ice Shelf and Ross Sea Regions of Antarctica. *J. Appl. Meteorol. Climatol.* **49**: 1306–1321, doi: 10.1175/2010JAMC2245.1.

Lazzara MA, Weidner GA, Keller LM, Thom JE, Cassano JJ. 2012a. Antarctic Automatic Weather Station Program. *Bull. Am. Meteorol. Soc*. **93**: 1519–1537, doi: 10.1175/BAMS-D-11-00015.1.

Lazzara MA, Keller LM, Markle T, Gallagher J. 2012b. Fifty-year Amundsen-Scott South Pole station surface climatology. *Atmos. Res.* **118**: 240–259, doi: 10.1016/j.atmosres.2012.06.027.

Marshall GJ. 2003. Trends in the southern annular mode from observations and reanalyses. *J. Clim.* **16**: 4134–4143, doi: 10.1175/1520-0442(2003)016<4134:TITSAM>2.0.CO;2.

Marshall GJ. 2007. Half-century seasonal relationships between the Southern Annular mode and Antarctic temperatures. *Int. J. Clim.* **27**: 373–383, doi: 10.1002/joc.1407.

Meehl GA. 1991. A reexamination of the mechanism of the semiannual oscillation in the Southern Hemisphere. *J. Clim.* **4**: 911–926, doi: 10.1175/1520-0442(1991)004<0911:AROTMO>2.0.CO;2.

Monaghan AJ, Bromwich DH, Powers JG, Manning KW. 2005. The climate of the McMurdo, Antarctica, Region as represented by one year of forecasts from the Antarctic mesoscale prediction system. *J. Clim.* **18**: 1174–1189, doi: 10.1175/JCLI336.1.

Nigro MA, Cassano JJ. 2014. Identification of surface wind patterns over the Ross Ice Shelf, Antarctica using self organizing maps. *Mon. Weather Rev.* **142**: 2361–2378, doi: 10.1175/MWR-D-13-00382.1.

Nigro MA, Cassano JJ, Lazzara MA, Keller LM. 2012. Case Study of a barrier wind corner jet off the coast of the Prince Olav Mountains, Antarctica. *Mon. Weather Rev.* **140**: 2044–2062, doi: 10.1175/MWR-D-11-00261.1.

Nylen TH, Fountain AG, Doran PT. 2004. Climatology of Katabatic winds in the McMurdo dry valleys, southern Victoria Land, Antarctica. *J. Geophys. Res.* **109**: D03114, doi: 10.1029/2003JD003937.

Parish TR, Cassano JJ, Seefeldt MW. 2006. Characteristics of the Ross Ice Shelf air stream as depicted in Antarctic Mesoscale Prediction System simulations. *J. Geophys. Res.* **111**: D12109, doi: 10.1029/2005JD006185.

Schwerdtfeger W. 1984. *Weather and Climate of the Antarctic, Developments in Atmospheric Science*, Vol. **15**. Elsevier: New York, NY.

Seefeldt MW, Cassano JJ. 2012. A description of the Ross Ice Shelf air stream (RAS) through the use of self-organizing maps (SOMs). *J. Geophys. Res.* **117**: D09112, doi: 10.1029/2011JD016857.

Seefeldt MW, Cassano JJ, Parish TR. 2007. Dominant regimes of the Ross Ice Shelf surface wind field during austral autumn 2005. *J. Appl. Meteorol. Climatol.* **46**: 1993–1955, doi: 10.1175/2007JAMC1442.1.

Simmonds I, Jones DA. 1998. The mean structure and temporal variability of the southern semiannual oscillation simulated in the GFDL coupled GCM. *Int. J. Climtol.* **18**: 473–504, doi: 10.1002/(SICI)1097-0088(199804)18:5<473::AID-JOC266>3.0.CO;2–0.

Simmonds I, Keay K. 2000. Mean Southern Hemisphere extratropical cyclone behavior in the 40-year NCEP–NCAR reanalysis. *J. Clim.* **13**: 873–885.

Stearns CR, Keller LM, Weidner GA, Sievers M. 1993. Monthly mean climatic data for Antarctic automatic weather stations. In *Antarctic Meteorology and Climatology: Studies Based on Automatic Weather Stations*. Antarctic Research Series No. 61, Bromwich DH, Stearns CR (eds). American Geophysical Union, Washington, DC, 1–21.

Steinhoff DF, Bromwich DH, Monaghan A. 2013. Dynamics of the Foehn mechanism in the McMurdo dry valleys of Antarctica from polar WRF. *Q. J. R. Meteorol. Soc.* **139**: 1615–1631, doi: 10.1002/qj.2038.

Turner J. 2004. The El Nino-southern oscillation and Antarctica. *Int. J. Climatol.* **24**: 1–31, doi: 10.1002/joc.965.

Turner J, Colwell SR, Marshall GJ, Lachlan-Cope TA, Carleton AM, Jones PD, Lagun V, Reid PA, Iagovkina S. 2005. Antarctic climate change during the last 50 years. *Int. J. Climatol.* **25**: 279–294, doi: 10.1002/joc.1130.

Turner J, Phillips T, Hosking JS, Marshall GJ, Orr A. 2013. The Amundsen Sea low. *Int. J. Climatol.* **33**: 1818–1829, doi: 10.1002/joc.3558.

Van den Broeke MR. 1998a. The semiannual oscillation and Antarctic climate, part 1: influence on near-surface temperatures (1957–1979). *Antarct. Sci.* **10**: 175–183.

Van den Broeke MR. 1998b. The semiannual oscillation and Antarctic climate, part 2: recent changes. *Antarct. Sci.* **10**: 184–191.

Van den Broeke MR. 2000. On the interpretation of Antarctic temperature trends. *J. Clim.* **13**: 3885–3889, doi: 10.1175/1520-0442(2000)013<3885:OTIOAT>2.0.CO;2.

Van Lipzig NPM, Turner J, Colwell S, Van den Broeke MR. 2004. The near-surface wind field over the Antarctic continent. *Int. J. Climatol.* **24**: 1973–1982, doi: 10.1002/joc.1090.

Van Loon H. 1966. The half-yearly oscillations in middle and high southern latitudes and coreless winter. *J. Atmos. Sci.* **24**: 472–486, doi: 10.1175/1520-0469(1967)024<0472:THYOIM>2.0.CO;2.

Welhouse L, Lazzara MA, Keller LM, Tripoli GJ, Hitchman MH. 2016. Composite analysis of the effects of ENSO events on Antarctica. *J. Clim.* (in press).

Wendler G, Kodama Y. 1993. The Kernlose winter in Adelie Coast. In *Antarctic Meteorology and Climatology: Studies Based on Automatic Weather Stations*. Antarctic Research Series No. 61, Bromwich DH, Stearns CR (eds). American Geophysical Union, Washington, DC, 139–147.

Wilson AB, Bromwich DH, Hines KM, Wang S. 2014. El Nino flavors and their simulated impacts on atmospheric circulation in the high southern latitudes. *J. Clim.* **27**: 8934–8955, doi: 10.1175/JCLI-D-14-00296.1.

Wolter K, Timlin MS. 1993. Monitoring ENSO in COADS with a seasonally adjusted principal component index. In *Proceedings of the 17th Climate Diagnostics Workshop*, Norman, OK, 52–57.